Composite Structures 358 (2025) 118982

Contents lists available at ScienceDirect

Composite Structures

journal homepage: www.elsevier.com/locate/compstruct

Mechanical and statistical analysis of hand-woven jute fibre composite laminates with bio-based and synthetic matrices

Paulo Victor de Assis [a,b], Rodrigo José da Silva [a,c,d,**], Guilherme Germano Braga [a], Antonio Carlos Ancelloti Junior [b], Marcio Eduardo Silveira [a], Tulio Hallak Panzera [a,*], Fabrizio Scarpa [c]

[a] Centre for Innovation and Technology in Composite Materials (CIT^{e}C), Federal University of São João del Rei (UFSJ), São João del-Rei, Brazil
[b] Núcleo de Tecnologia em Compósitos (NTC), Federal University of Itajubá (UNIFEI), Itajubá, Brazil
[c] Bristol Composites Institute, School of Civil, Aerospace and Design Engineering (CADE), University of Bristol, Bristol, United Kingdom
[d] CERN, the European Organization for Nuclear Research, R&D Programme EP-DT, Geneva, Switzerland

ARTICLE INFO

Keywords:
Composites
Jute fabrics
Castor oil
Mechanical properties
Finite element analysis

ABSTRACT

This study describes the use of continuous jute yarn fabrics innovatively manufactured through manual loom, followed by a hand lay-up process to obtain composite laminates with biobased castor oil and epoxy systems. A full factorial design (2^2) is employed to evaluate the effects of matrix phases (epoxy and castor oil polymers) and jute fibres (uni- and bidirectional fabrics) on the apparent density, porosity, tensile, three-point bending, and Charpy impact responses. The three-point bending behaviour is also predicted through numerical simulations using a finite element numerical analysis to validate the elastic behaviour of the laminates. The incorporation of castor oil matrix results in decreased density, tensile modulus, flexural strength, and flexural modulus, while simultaneously increasing the porosity and the impact resistance compared to the epoxy laminates. Additionally, unidirectional fabrics have lower porosity and enhanced mechanical properties in the longitudinal direction compared to bidirectional reinforcements. Overall, these composites appear to be sustainable and cost-effective alternatives for use within secondary structural design applications.

1. Introduction

Sustainability has driven recent developments in technology, leading to innovations that meet environmental, social and economic goals. This growing understanding of sustainability issues has encouraged researchers and engineers to develop materials and processes that reduce waste and carbon footprints, promoting resource efficiency. Biobased polymers and natural fibres in composite materials demonstrate how sustainability-driven requirements can lead to technological advancements that meet industry demands while minimising ecological impacts. These developments are crucial to address global challenges such as climate change and resource depletion. The development of sustainable materials is essential for balancing economic viability, social benefits, and environmental sustainability. Eco-friendly materials have the potential to reduce costs, create job opportunities, and significantly lower environmental impacts, thus supporting the three pillars of sustainability [1–3].

Fully biobased composites can be used as environmentally friendly solutions for several industrial applications in sectors such as automotive, civil, and aeronautics [4]. Research and development have proven that natural fibres have been successfully applied as reinforcements in composites. Among the large quantity of fibre plants available in nature, some of the most common in bio-composites are bamboo, banana, corn, cotton, flax, hay, hemp, jute, kenaf, pineapple leaf, ramie, sisal, and sugar palm [3]. Continuous natural fibres such as jute fabrics enable the possibility of producing large-scale products in different sizes and for multiple purposes of use. Therefore, several studies have been conducted to investigate the potential of using jute fabrics in polymer composites [5,6], but only a few works have assessed the mechanical performance of unidirectional jute fabric composites [7–10].

Flores et al. [9] conducted physical and mechanical tests to examine the impact of hybridisation on the properties of laminates made from

* Corresponding author at: UFSJ.
** Corresponding author at: CERN.
E-mail addresses: rjs.phd@cern.ch (R.J. da Silva), panzera@ufsj.edu.br (T.H. Panzera).

https://doi.org/10.1016/j.compstruct.2025.118982
Received 27 August 2024; Received in revised form 23 December 2024; Accepted 14 February 2025
Available online 16 February 2025

Table 1
Properties of the epoxy and castor oil systems.

Property	Epoxy polymer 956 [20]	Castor oil polymer [16]
Apparent density (g/cm^3)	1.170 ± 0.001	0.88 ± 0.07
Tensile strength (MPa)	42.8 ± 2.5	5.50 ± 0.50
Tensile modulus (GPa)	1.92 ± 0.11	0.30 ± 0.01
Flexural strength (MPa)	67.9 ± 1.4	7.60 ± 0.06
Flexural modulus (GPa)	1.86 ± 0.09	0.33 ± 0.01
Impact Resistance (kJ/m^2)	8.7 ± 1.4	16.60 ± 1.50

unidirectional jute, E-glass, and carbon fabric reinforcements, using polyester resin as the matrix. The authors reported tensile and flexural strengths of 571 MPa and 204 MPa, respectively. In a separate study, Devireddy and Biswas [10] fabricated and assessed the properties of unidirectional banana/jute hybrid fibre-reinforced epoxy composites, achieving optimal results of 64.75 MPa for tensile strength and 104.24 MPa for flexural strength. They noted that the presence of porosity and voids increased significantly when the fibre loading exceeded 30 wt%, which adversely affected the tensile and flexural strengths.

Despite the increased use of natural fibres in composites, most researchers have primarily focused on using these fibres to reinforce petroleum-based polymers [3]. In contrast, castor oil polyurethane has been explored over the years as a viable alternative to synthetic polymers. One of the key advantages of castor oil polyurethane (PU) is that it does not compete with the food industry, as it is non-edible [11]. This Bio-PU has served as the matrix phase for innovative composites made from sisal and coir fibres [12,13], *Cynodon spp*. (grass fibres) [14], as well as glass and aramid fibres [15]. Additionally, it has been used as an adhesive for sandwich structures featuring bamboo ring cores [16,17] and recycled bottle caps [18]. Moreover, numerical assessments have proven to be an effective approach for evaluating novel eco-friendly alternative materials [17–19].

To the best of the authors' knowledge, this study represents the first attempt to produce and characterise a fully bio-based composite made from jute fabric and castor oil polyurethane, using a manufacturing process that includes fabrics produced on a manual loom, making it suitable for large-scale production and diverse component sizes. Jute fibre yarns (ropes) are arranged into unidirectional and bidirectional fabrics, which are the processed using a hand lay-up technique. Additionally, laminates with a non-sustainable epoxy matrix are produced for comparison. Four experimental conditions are evaluated across tensile, three-point bending, and Charpy impact testing, as well as apparent density and porosity measurements. The results are rigorously compared using statistical analysis. Additionally, a nonlinear implicit and incremental numerical simulation is employed to enhance the understanding of the bending behaviour of the composites.

2. Materials and methods

2.1. Materials

The epoxy system, sourced from Huntsman (Brazil), consists of Renlam M and hardener HY956 mixed at a 5:1 (wt/wt) ratio. Castor oil-based polyurethane (AGT 1315), supplied by *Imperveg* (Brazil), is a two-component adhesive, comprising a pre-polymer (component A) and a polyol (component B) mixed at a 1:1.2 (wt/wt) ratio. The physical and mechanical properties of such polymers are presented in Table 1, sourced from other publications within the same research group and batches. The castor oil-based polymer exhibits lower apparent density and higher impact resistance, whereas the epoxy polymer demonstrates superior static mechanical properties under tensile and flexural loadings.

Twisted jute yarns with a diameter of approximately 0.83 mm (± 0.09) serve as the raw material, which are woven on a manual loom (Fig. 1a and 1b) to create unidirectional (Fig. 1c) and bidirectional (Fig. 1d) jute fabrics. The jute fabrics are subsequently cut into 220 × 220 mm^2 pieces and pre-stressed with 5 mm wide double-sided tape to ensure proper alignment of the yarns. Both unidirectional (UD) and bidirectional (BD) fabrics have similar grammages with mean values of 431.8 ± 3.7 g/m^2 and 433.9 ± 5.5 g/m^2, respectively. This similarity is intentionally achieved through the fabrication process. The manual loom enables control over the spacing of the yarns in both directions. For both unidirectional (UD) and bidirectional (BD) fabrics, the same fibre amount per unit area is maintained. In the bidirectional fabric, the spacing between the continuous yarns in each direction is twice that of the spacing in the unidirectional fabric. Consequently, fabrics with equivalent grammage are obtained. The motivation for comparing UD and BD composite laminates with the same fibre amount arises from the fact that the UD architecture offers greater stiffness and strength along the fibre direction but exhibits significant anisotropy. In contrast, the BD configuration may present lower stiffness and strength but reduces anisotropy in the 1–2 plane due to a balanced fibre distribution. Insights

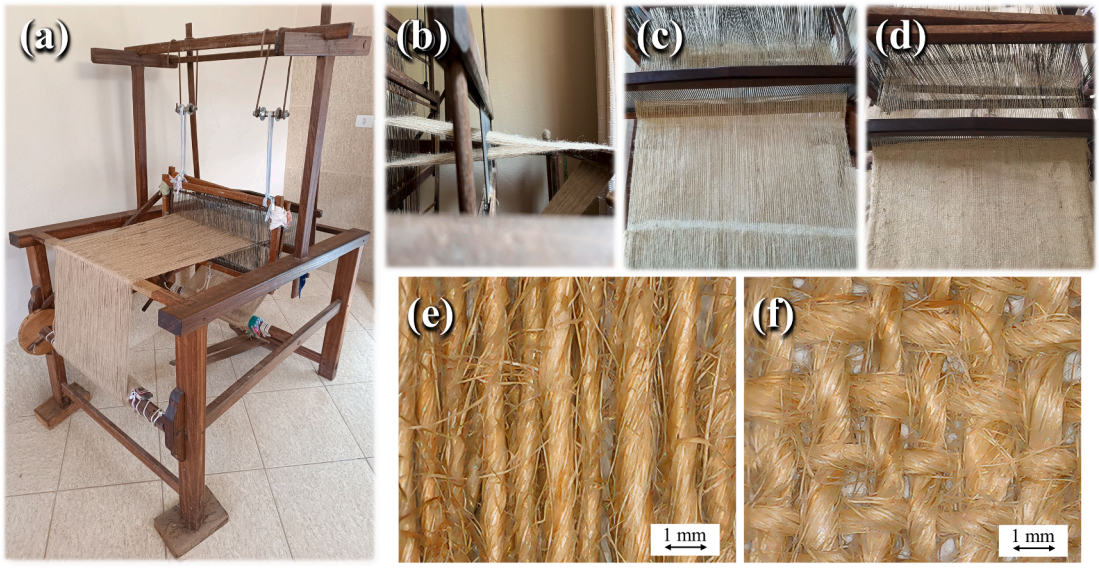

Fig. 1. (a) The manual loom; (b) yarns spliced on the manual loom; manufacturing of the (c) UD and (d) BD jute fabrics; and insight on the architecture of (e) UD and (f) BD jute fabrics.

Table 2
Full factorial design 2^2.

Experimental condition	Matrix phase	Reinforcement
1	Epoxy	Unidirectional fabric (UD)
2	Epoxy	Bidirectional fabric (BD)
3	Castor oil	Unidirectional fabric (UD)
4	Castor oil	Bidirectional fabric (BD)

into the fabric architectures of UD and BD types are illustrated in Fig. 1e and Fig. 1f, respectively. The UD fabric contains approximately 12 aligned yarns per cm^2, while the BD fabric features 6 yarns in each direction.

2.2. Design of experiments (DoE)

The Design of Experiment (DoE) is a statistical method used to investigate the influence of various factors within an experiment, evaluating both their individual effects, especially, their interactions [21]. DoE is widely applied across numerous disciplines, including the physical and mechanical evaluation of materials and structures [12–18]. A 2^2 full factorial design is employed to analyse the impact of the matrix phase type (epoxy and castor oil polymer) and reinforcement phase (uni- and bidirectional fabrics) on the physical and mechanical properties of jute fibre composites, resulting in four experimental conditions outlined in Table 2. Certain parameters including the number of fibre layers per composite plate (2 layers), the uniaxial pressure (654 kPa), the cold-pressing time (22 h), and the curing time (14 days), are maintained constant. The response variables are apparent density, apparent porosity, tensile modulus and strength, modulus of toughness, flexural modulus and strength and impact resistance. For each of the four proposed tests and four experimental conditions, five specimens per replicate are considered, resulting in a total of 160 specimens. Two replicates are used in this process. The Design of Experiments (DoE) and Analysis of Variance (ANOVA) techniques are conducted using Minitab™ v.21 statistical software. To minimise the influence of uncontrolled factors on the responses, a randomisation procedure is implemented during sample fabrication and testing.

2.3. Manufacturing process

The composite materials undergo a multi-step fabrication process. A hand lay-up technique is used, followed by cold uniaxial compaction using a metal mould measuring 220 × 220 mm^2. Initially, inside the mould, an aluminium plate is positioned and covered with a thin layer of wax as a release agent to ensure a smooth surface finish. The jute fabrics (BD or UD) are then added to the mould (Fig. 2a), and the matrix material (epoxy or castor oil) is applied over the fibres. The laminates, with a thickness of approximately 2.1 mm (± 0.2), are designed to achieve a fibre volume of 30 %. Consequently, the hand lay-up process requires the application of a specific amount of polymer. The quantity of the matrix is estimated based on the apparent densities of both the fibre and matrix phases. The bicomponent polymer systems are prepared by hand-mixing for 5 min at room temperature, following the respective mixture ratios previously reported in Section 2.1. After spreading the liquid polymer over the fibres, a cold pressure of 654 kPa [4] is applied to compact the composite laminates (Fig. 2b), which are subsequently removed from the mould after 22 h under pressure (Fig. 2c). The

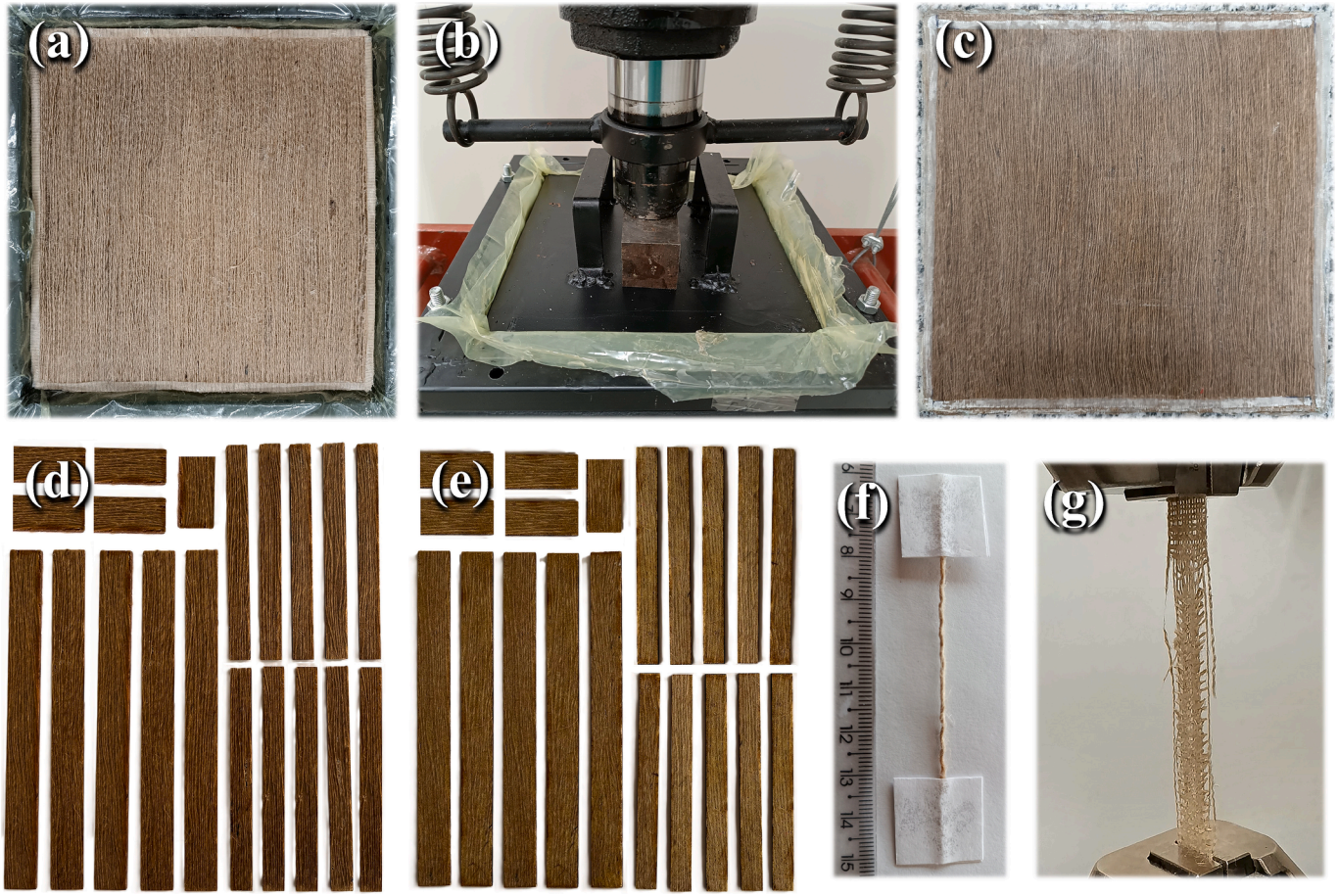

Fig. 2. The manufacturing process of the composite laminates: (a) lay-up, (b) compaction, (c) demoulding, (d) epoxy UD specimens, (e) castor oil UD specimens, (f) jute yarn, and (g) jute fabric specimen.

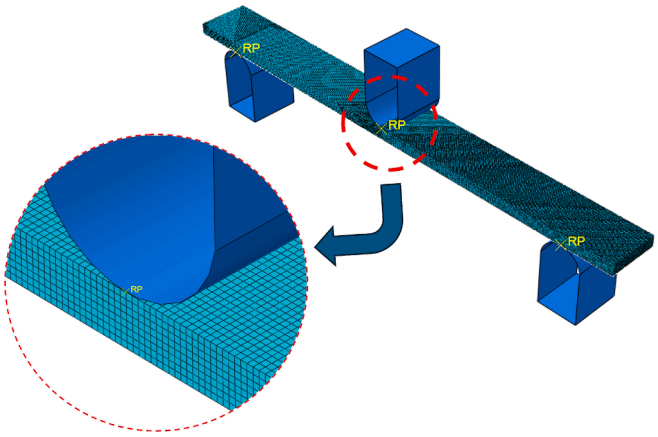

Fig. 3. A finite element numerical model for assessing the elastic behaviour of the composite laminates under three-point bending.

compaction and curing of the composites take place in an environment with controlled conditions (23°C and 55 % relative humidity). Finally, a CO_2 laser cutting machine (Robotech 150 W) is used to obtain samples with dimensions in accordance with ASTM standards recommendations (Fig. 2d and 2e). The UD laminate specimens are subjected to three-point bending testing in two configurations, with the load applied either parallel or perpendicular to the fibre direction. Nevertheless, the transverse elastic properties of UD composites are expected to be predominantly influenced by the matrix phase [22, p. 51], closely resembling those observed in previous tests conducted on the polymer materials (Table 1). The transverse properties of UD composites, while not the primary focus of the statistical approach, are essential for the accurate development of FEA models proposed further in the text. Concerning the BD laminates, given their symmetry in both directions, they are tested solely in a single direction.

2.4. Mechanical characterisation of jute yarn and fabrics

The tensile properties of the jute fibre yarn are evaluated according to ASTM D3822-14 [23] standards. Two-sided paper is fixed to the edges of 90 mm jute yarns (Fig. 2f), resulting in a 50 mm gauge length. Twenty specimens undergo testing at a rate of 2 mm/min using an Instron machine equipped with a 1 kN load cell. The assumption of constant cross-sections of the yarns is made to estimate their tensile properties. Additionally, the apparent density of the jute fibre is determined using the Archimedes principle. The samples are water-saturated inside a desiccator under vacuum for 24 h. Furthermore, the tensile characteristics of eight specimens of both uni- and bidirectional jute fabrics are evaluated at a rate of 2 mm/min using a Shimadzu AG-X Plus machine fitted with a 100 kN load cell (Fig. 2g). The specimens measure 200 mm in length and 25 mm in width. Fiberglass laminates, sized 25 mm by 25 mm, serve as tab material, establishing a gage length of 150 mm.

2.5. Characterisation of the composite laminates

The composite samples are characterised using tensile and three-point bending tests following the ASTM D3039-17 [24] and ASTM D790-17 [25] standards, respectively. Tensile testing is performed at a rate of 2 mm/min using a Shimadzu AG-X Plus machine (100 kN), with a gauge length of 100 mm in specimens with dimensions of 150 × 15 × 2.1 mm^3. The three-point bending testing is performed using an Instron machine (1 kN), by 80 mm in the support span length for specimen dimensions of 100 × 9.81 × 2.1 mm^3. Additionally, Charpy impact tests are carried out across the flatwise direction in 100 × 10 × 2.1 mm^3 specimens with a span of 60 mm, following ASTM D6110-18 [26], using an impact hammer tester XJJ Series. The apparent density and apparent porosity are determined using Archimedes' principle as per BS EN ISO 10545–3 [27]. The specimens (32 × 20 mm^2) are saturated using distilled water and a desiccator coupled to a vacuum pump. Measurements of m_1 (dry mass), m_2 (impregnated mass), and m_3 (impregnated and suspended mass) are obtained using a precision scale (0.001 g). The apparent density is calculated by dividing m_1 by ($m_1 - m_3$), and the

Fig. 4. (a) Three-point bending test for the transverse castor oil composite and (b) tensile test in the ± 45° epoxy composite.

Table 3
Mechanical properties of the UD laminates applied in finite element analysis.

Property	Composite architecture UD epoxy	UD castor oil
E_1 (GPa)	6.99	4.60
E_2 and E_3 (GPa)	1.82	0.39
Nu_{12} and Nu_{13}	0.42	0.37
Nu_{23}	0.34	0.28
G_{12} and G_{13} (GPa)	0.56	0.31
G_{23} (GPa)	0.68	0.15

apparent porosity is determined by dividing $(m_2 - m_1)$ by $(m_2 - m_3)$.

2.6. Finite element analysis

A numerical model (Fig. 3) is validated using finite element analysis (FEA) in ABAQUS software, focusing on an elastic-only analysis to predict the force–displacement behaviour of the UD composite laminates under bending. The selection of UD laminates was driven by their simplified anisotropic structure, which facilitates a clearer understanding of the material's response to bending loads and provides a robust basis for future investigations into more complex laminate configurations. The emphasis is on the elastic regime, as materials and structures are typically designed to operate within this range, ensuring predictable and reversible deformation. The bending test is chosen due to its more complex loading nature, involving compression above the neutral axis and tension below, which provides a comprehensive understanding of the material's response. Simulations are conducted on a three-dimensional extruded body with dimensions corresponding to the three-point bending specimens ($100 \times 9.81 \times 2.1$ mm^3), using hexahedral 3D stress elements for the analysis. The mesh elements are oriented to align with the top face of the laminate (the surface in contact with the loading indenter), treating this surface as the top face of the mesh. Cylindrical indenters with a diameter of 8 mm are modelled as Analytical Rigid Surfaces, to represent the loading apparatus and support span tools, which are separated by 80 mm. The contact interactions between the indenters (defined as the master surface) and the laminate (defined as the slave surface) are established using the node-to-surface discretisation method. For normal contact behaviour, a "hard" contact condition is applied, while a friction coefficient of 0.20 is introduced for tangential contact behaviour to account for sliding resistance, based on [28]. The central deflection (displacement) is set as 2.5 mm, representing an appropriated range for the elastic regime, in line with experimental data. The simulation is executed using the "Static, General" step, which includes automatic stabilisation through a specific dissipated energy fraction of 0.0002, with a maximum allowable ratio of dissipated energy to strain energy set at 0.05 (ABAQUS standard setup).

To ensure the composite nature of the laminates, the mechanical properties are defined through the engineering constants: E_1, E_2, E_3, Nu_{12}, Nu_{13}, Nu_{23}, G_{12}, G_{13}, and G_{23}. In ABAQUS nomenclature, "E" denotes the elastic modulus, "Nu" represents the Poisson ratio, and "G" indicates the shear modulus. Following well-established concepts for composite laminates, several assumptions are made: E_1 is considered the flexural modulus of the laminate; $E_2 = E_3$ is the elastic modulus measured under three-point bending in the transverse direction [22, p. 76], as depicted in Fig. 4a; $Nu_{12} = Nu_{13}$ is the Poisson ratio of the laminate, measured through a tensile test in the fibre direction [22, p. 76] using a video-gage system coupled to the universal testing machine; and Nu_{23} is assumed as the Poisson ratio of the matrix material, by considering the matrix dominance in the transverse direction of UD composites [22, p. 51]. The in-plane shear constants are assumed identically for UD composites [22, p. 76], therefore $G_{12} = G_{13}$ is measured by tensile testing under the same parameters as the previously reported tensile tests, with the UD fibres aligned in $\pm 45^\circ$ to the tensile loading, based on the ASTM D3518 standard [29], as depicted in Fig. 4b. Finally, G_{23} is determined using the equation $E_2/(2(1 + Nu_{23}))$, based on [22, p. 54]. Table 3 presents all these mechanical properties applied in finite element analysis, with the transverse modulus being close to those indicated in Table 1 for the matrix phase.

Table 4
Example of mesh convergence – UD epoxy laminate.

Interaction	Mesh size (mm)	Elements inthickness	Totalelements	Force (N)	Variation in forcefrom (n) to (n + 1)
n = 1	1.0500	2	1728	9.34	–
n = 2	0.5250	4	14,440	11.89	27 %
n = 3	0.3500	6	48,048	12.45	5 %
n = 4	0.2625	8	112,480	12.57	1 %

The mesh size is determined using a convergence method based on the number of mesh elements across the thickness. Initially, two elements are used in the thickness, corresponding to a mesh size of 1.05 mm, which is half of the laminate thickness (2.1 mm). The number of elements in the thickness is then increased (mesh refinement) in multiples of two to ensure that nodes always discretize the neutral axis under bending. As a stopping criterion, it is established that the measured force for a 2.5 mm displacement in a given mesh condition should be less than 5 % of the value measured for the previous (coarser) mesh. An example of mesh convergence for the UD epoxy laminate is presented in Table 4. The optimal mesh size for both configurations (epoxy and castor oil matrix composites), according to the proposed stopping criteria, is 0.2625 mm, which corresponds to 8 elements in the laminate thickness and a total of 112,480 hexahedral elements.

3. Results and discussion

3.1. Jute fibre yarn and fabrics

Table 5 presents the physical and mechanical properties of the pristine jute yarns, as well as the UD and BD fabrics. Fig. 5a illustrates the tensile strength and modulus values of jute yarns, which are consistent with those reported in the literature [28,29]. Notably, these values are nearly ten times lower than those documented for a single jute filament [30–35]. A single jute filament may demonstrate greater strength than multiple filaments twisted into a yarn, as it allows for more effective load transfer along its length. In contrast, when filaments are twisted into a yarn, their orientation becomes significantly less uniform with respect to the loading direction, resulting in stress concentration and lower stress distribution.

The tensile data for the fabrics are estimated using two approaches: (i) the area of yarns aligned along the loading direction and (ii) the homogenised area of the fabric. In the yarn area methodology, the area for stress calculation is determined by multiplying the number of yarns parallel to the loading direction by the area of a single yarn. In contrast, the homogenised methodology estimates the area for stress calculation by multiplying the width of the fabric by its thickness, which roughly corresponds to the diameter of the yarns. The stress–strain behaviours for UD and BD fabrics using the yarn area approach are illustrated in Fig. 5b and 5c, respectively, while the homogenised approach is shown in Fig. 5d and 5e. Analysing the yarn methodology reveals that UD and BD fabrics exhibit similar tensile strength and modulus. Although the UD fabric can bear approximately twice the load of the BD fabric, it also has double the yarn area, which contributes to this similarity. In the homogenised methodology, UD fabrics outperform BD fabrics, as the homogenised area remains consistent for both configurations.

BD fabrics display a more pronounced toe region in the tensile curves (Fig. 5c and 5e) compared to UD fabrics (Fig. 5b and 5d) due to their structural composition. In BD fabrics, the yarns are arranged in two directions, facilitating greater interaction and friction between the fibres during initial loading. This results in a more gradual engagement of the fibres, leading to an extended toe region where the fabric stretches

Table 5
Physical and mechanical properties for the jute fibre yarn and fabrics.

Property	Jute yarns	UD jute fabric (yarns' area)	BD jute fabric (yarns' area)	UD jute fabric (homogenised)	BD jute fabric (homogenised)
Diameter * (μm)	688–976	–			
Apparent density (g/cm^3)	1.359–1.362	**			
Tensile strength (MPa)	59.63–97.99	44.14–56.51	48.54–58.88	27.80–38.13	16.44–21.05
Modulus of elasticity (GPa)	2.71–5.52	2.88–3.94	1.94–3.45	1.85–2.66	0.84–1.19

*Measured through optical microscopy.
** Grammage of about 433 g/m^2.

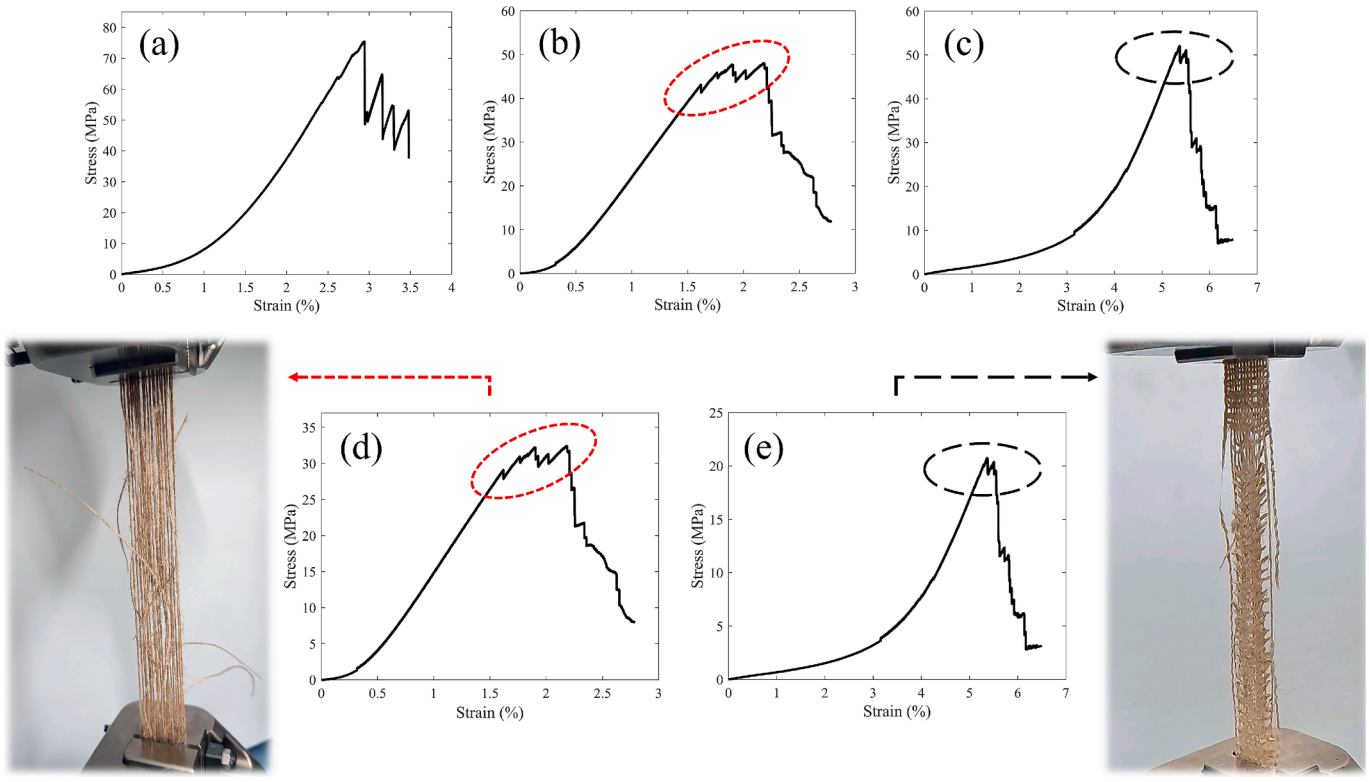

Fig. 5. Typical tensile stress/strain curves for the (a) single jute fibre yarn, (b) UD fabric, (c) BD fabric, (d) UD and (e) BD through the homogenised concept.

Table 6
Physical and mechanical properties of the laminates.

Property	Composite architecture UD epoxy	UD castor oil	BD epoxy	BD castor oil
Apparent density (g/cm^3)	1.187 ± 0.018	0.805 ± 0.024	1.183 ± 0.011	0.857 ± 0.012
Apparent porosity (%)	3.50 ± 0.84	3.77 ± 0.76	3.94 ± 0.80	4.15 ± 0.47
Tensile strength (MPa)	98.76 ± 6.97	65.02 ± 7.58	44.43 ± 5.33	33.67 ± 1.99
Tensile modulus (GPa)	6.70 ± 0.83	5.87 ± 0.39	3.87 ± 0.53	2.61 ± 0.15
Modulus of toughness (MJ/m^3)	1.61 ± 0.18	1.06 ± 0.16	0.74 ± 0.15	0.62 ± 0.08
Flexural strength (MPa)	87.97 ± 7.93	46.28 ± 7.27	54.15 ± 7.61	24.40 ± 1.99
Flexural modulus (GPa)	6.99 ± 0.79	4.60 ± 0.80	3.62 ± 0.60	1.63 ± 0.16
Impact resistance (kJ/m^2)	15.39 ± 1.80	19.63 ± 3.42	9.18 ± 0.53	18.83 ± 3.28

before achieving maximum alignment. Regarding failure behaviour, BD fabrics experience fewer yarn ruptures along the loading direction compared to UD fabrics (see the failures in Fig. 5). Although the shear effects caused by the transverse fibres may diminish the tensile properties of the composite laminate, this interaction appears to contribute to a reduced number of yarn ruptures within the fabric itself. This can be attributed to the transverse yarns absorbing energy and alleviating stress concentration on the longitudinal yarns through their interlocking points, thereby minimising ruptures. The increased number of yarn

Table 7
Analysis of Variance (ANOVA, P-value ≤ 0.05)).

Experimental factors	Main Factors Matrix Phase (MP)	Reinforcement Phase (RP)	Interactions MP × RP	R^2-adj
Apparent density	0.000	0.013	**0.007**	99.83 %
Apparent porosity	**0.021**	**0.003**	0.660	87.93 %
Tensile strength	0.003	0.000	**0.030**	96.62 %
Tensile modulus	**0.002**	**0.000**	0.517	97.25 %
Modulus of toughness	0.004	0.000	**0.015**	96.38 %
Flexural strength	**0.002**	**0.005**	0.283	92.44 %
Flexural modulus	**0.001**	**0.000**	0.512	96.57 %
Impact resistance	**0.004**	**0.038**	0.174	85.99 %

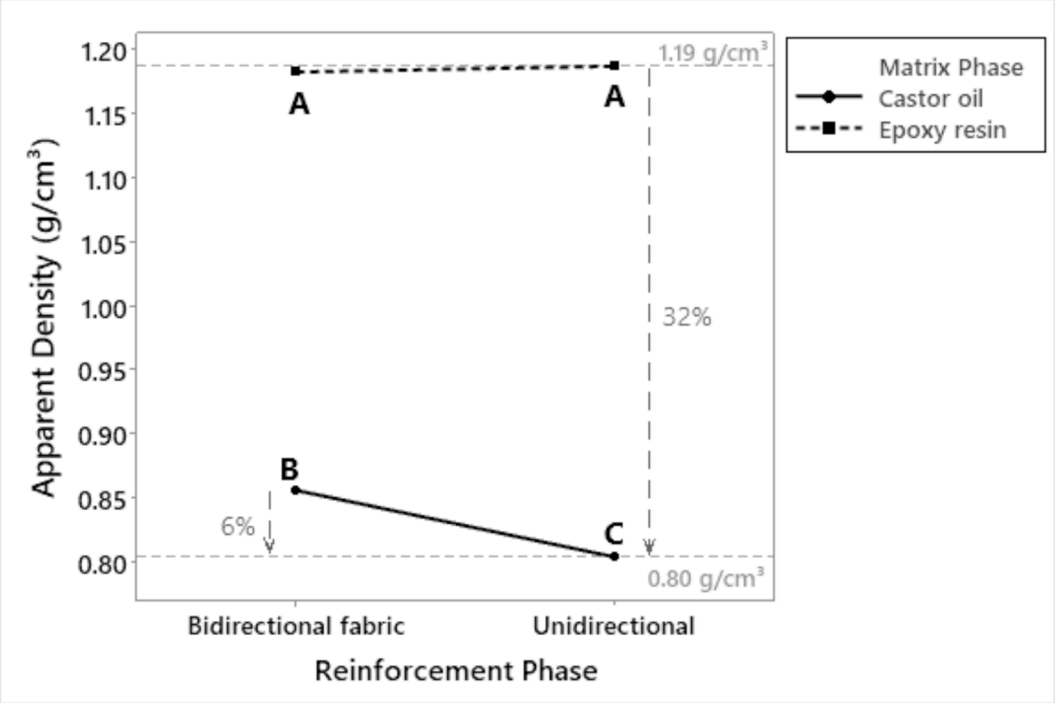

Fig. 6. Second-order interaction effect plot for the mean apparent density response.

ruptures in UD fabrics relative to BD fabrics is evident in the stress–strain curves (Fig. 5b, 5c, 5d, and 5e), particularly highlighted by the intermittent drops in stress within the maximum load region, indicated by dashed ellipses.

3.2. Statistical analysis

Table 6 presents the global mean and standard deviation for the physical and mechanical properties measured across all composite architectures, including the two replicates from the DoE approach. Table 7

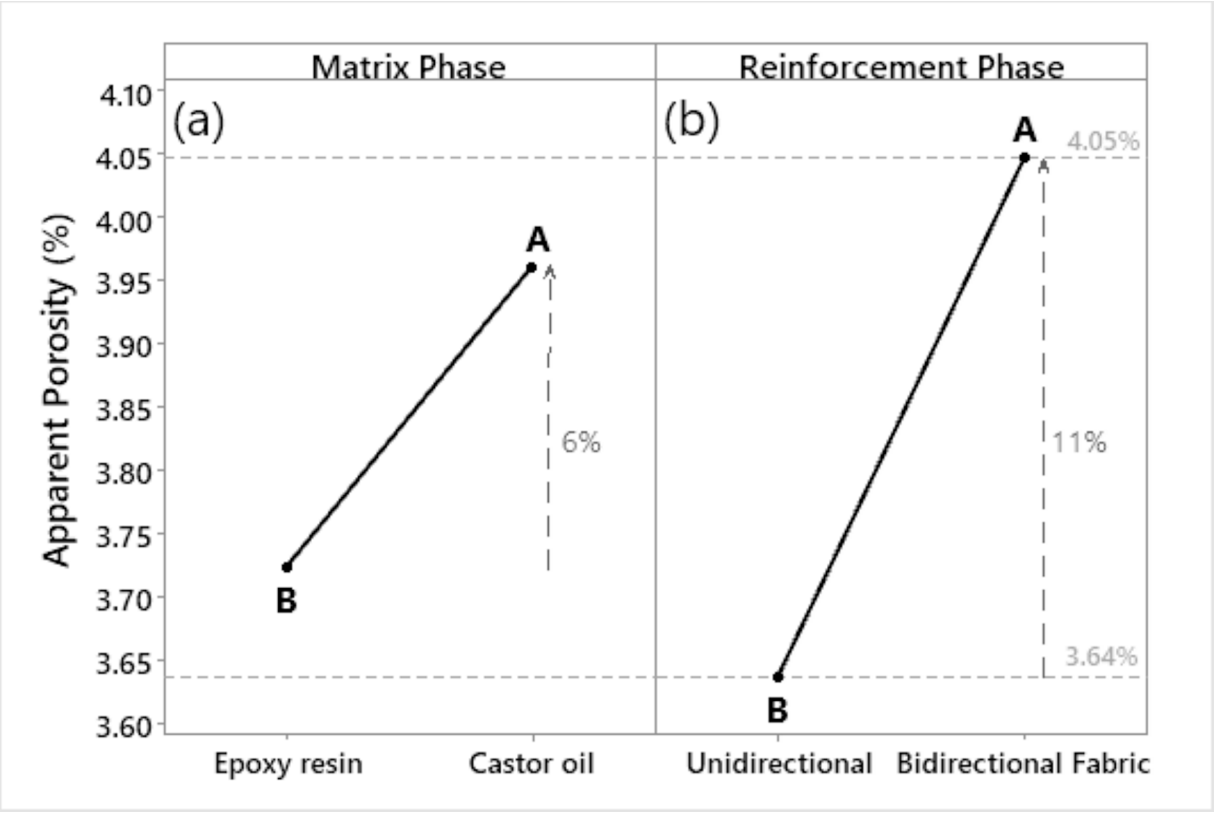

Fig. 7. Main effect plots of the mean apparent porosity: factors (a) matrix phase and (b) reinforcement architecture.

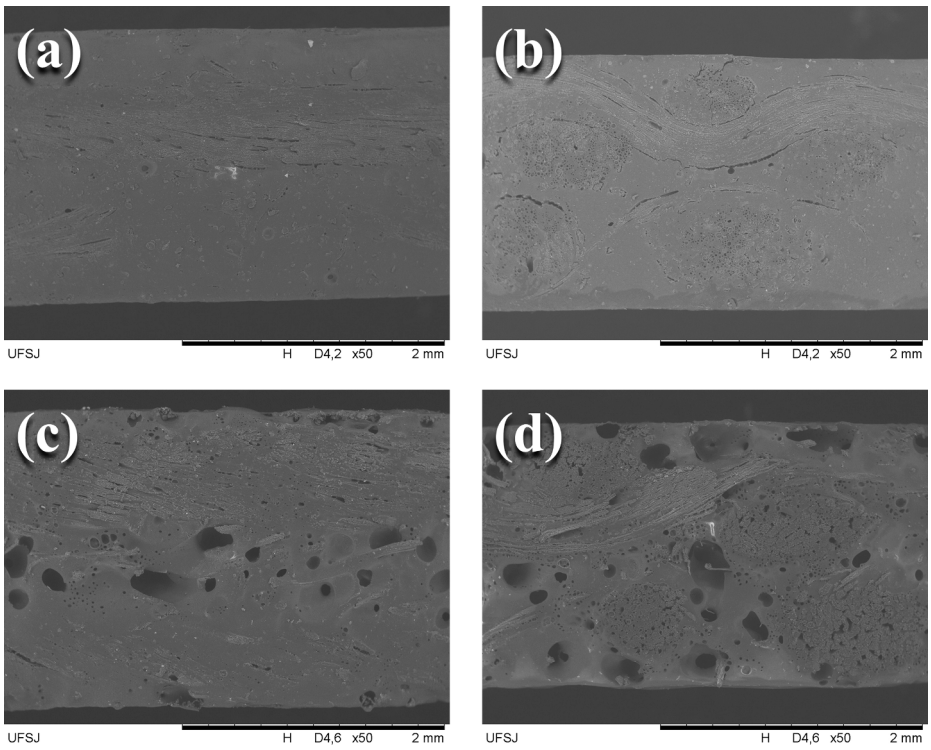

Fig. 8. SEM images of (a) UD and (b) BD epoxy composites; and (c) UD and (d) BD castor oil composites.

provides the Analysis of Variance (ANOVA) for the full factorial design used to evaluate the composite laminates. ANOVA is a statistical technique employed to determine whether the effects of different factors and/or their interactions on the response variables are statistically significant [21]. In this study, significance is assessed using the P-value, which indicates the probability that the observed effect could occur by chance. A P-value less than or equal to 0.05 signifies a statistically significant effect, suggesting that the factor or interaction has a meaningful influence on the material's performance. This analysis aids in identifying the key factors and their interactions that impact the behaviour of the composite materials. The main effect will only be interpreted in the absence of evidence of interactions between factors. P-values less than 0.05 are underlined in Table 7, with those in bold to be further interpreted through effect plots. Furthermore, a Tukey test is conducted in conjunction with the significant effect plots to compare the mean data between each experimental level, in which equal letter groups will indicate equivalent mean data. The adjusted R^2 values range from 85.99 % to 99.83 %, signifying a strong fit of the data to the

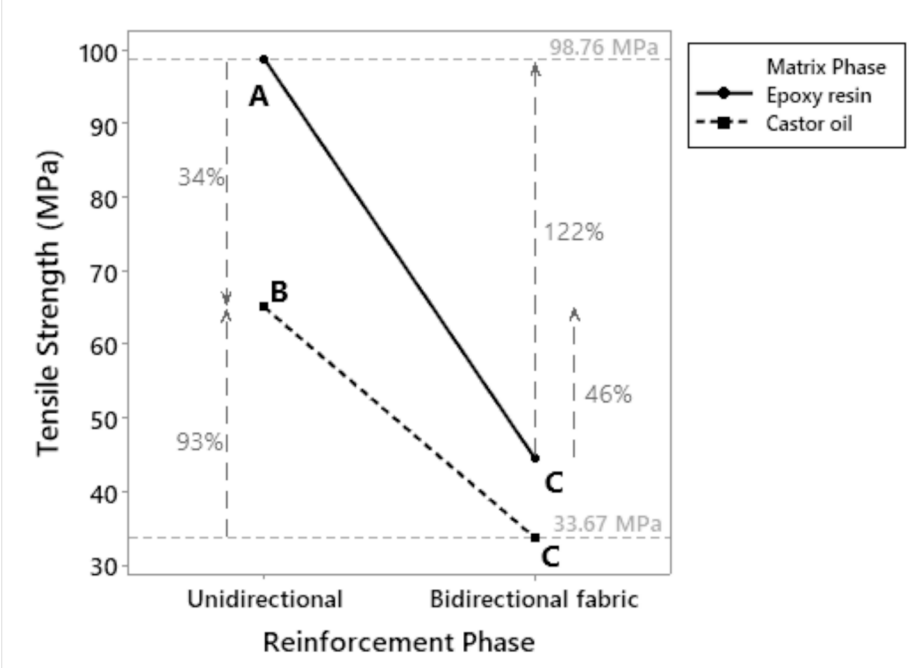

Fig. 9. Second-order interaction effect plot for the mean tensile strength response.

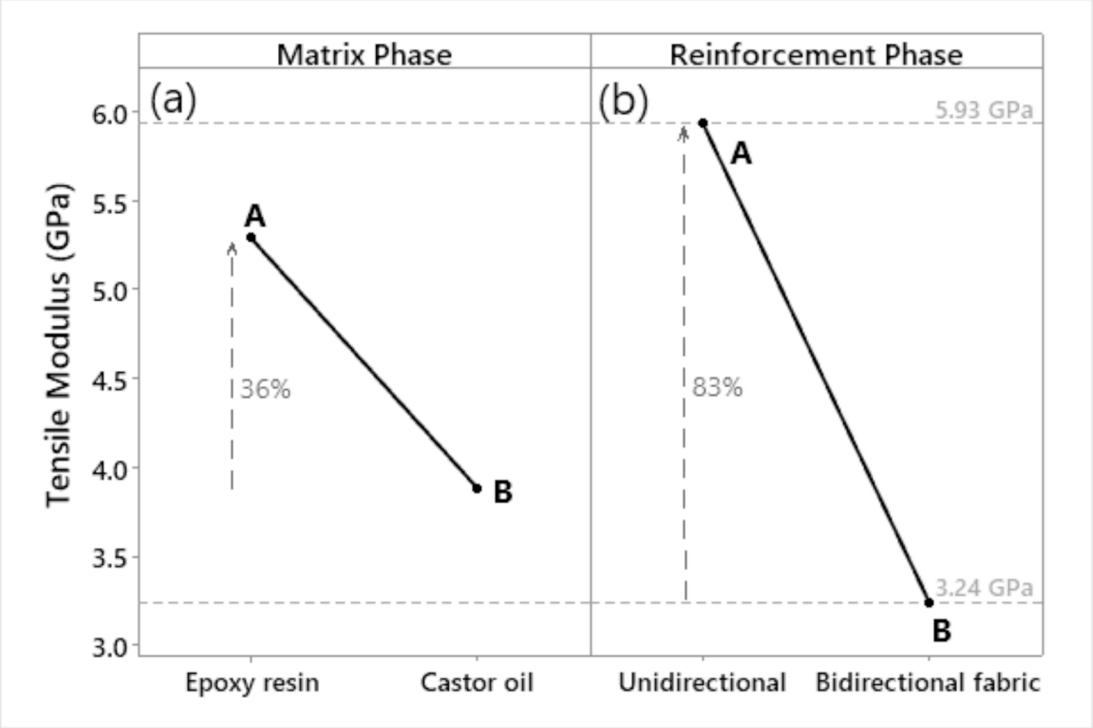

Fig. 10. Mean tensile modulus: effect plots of the (a) matrix and (b) reinforcement phases.

regression equation and indicating high predictability within the models.

3.2.1. *Apparent density*

The second-order interaction effect plot for the mean apparent density response, which varies from 0.80 to 1.19 g/cm^3, is shown in Fig. 6. The bold letters (A, B, and C) for each experimental condition represent the results of Tukey's comparison test, where identical letters indicate equivalent means. For non-identical means, the difference is expressed as a percentage. The castor oil matrix phase notably reduces the apparent density of the composite materials by about 32 %. This reduction is attributed to the significant disparity between the densities of the castor oil (0.88 g/cm^3) and epoxy (1.17 g/cm^3) systems, as previously presented in Table 1. Furthermore, Tukey's test reveals that the castor oil composites manufactured with UD jute yarns (Group C) exhibit lower density compared to those composed of BD fabric (Group B). Given that the fibre volume ratio is consistent between both UD and BD configurations, it is reasonable to attribute this minor variation (only 6 %) to the inherent bubble formation during the curing process of castor oil resin [12]. These bubbles tend to accumulate in the cross-yarn regions of the bidirectional fabrics.

3.2.2. *Apparent porosity*

Fig. 7 shows the main effect plots related to the mean apparent porosity response, ranging from 3.64 to 4.05 %. Composites with castor oil polymer exhibit about 6 % higher porosity than those with epoxy (Fig. 7a). As previously reported regarding density reduction, the increase in porosity is attributed to the intrinsic formation of bubbles that occur during the curing process of the castor oil resin [12]. In BD laminates, there is a greater tendency for bubbles to accumulate in the cross-yarn regions of the fabrics, resulting in an approximately 11 % increase in porosity compared to UD laminates (as shown in Fig. 7b).

The longitudinal sections of the composites are observed using a Hitachi TM-3000 tabletop SEM. Fig. 8 shows SEM images of epoxy (a, b) and castor oil (c, d) uni- and bidirectional fibre composites at 50 × magnification. Notably, internal macro pores are observed in the castor oil composites (Fig. 8c and Fig. 8d), particularly in those manufactured with BD fabrics (Fig. 8d). The macro pores observed via SEM confirm the porosity results shown in Fig. 7, and are consistent with the SEM results reporting bubbles within the castor oil polymer in [12].

3.2.3. *Tensile strength, modulus of elasticity, and modulus of toughness*

Fig. 9 illustrates the second-order interaction effect plot for the mean tensile strength of the composites, which varies from 33.67 to 98.76 MPa. The bidirectional fibre orientation leads to a reduction in tensile strength for both matrix phases. Conversely, an increase of up to 122 % is achieved when considering UD jute fibres. The highest strength is attained for UD jute fibres combined with the epoxy polymer, which also exhibits a lower porosity level (Fig. 8). Notably, the castor oil UD polymer-based samples demonstrate a 34 % reduction in strength compared to epoxy UD jute-reinforced composites. It is worth noting that castor oil UD fibre laminates (Group B) have an almost 46 % superior performance compared to BD fibre epoxy composites (Group C). Moreover, the composite laminates with BD architecture have the same strength under tensile, apart from the matrix type (epoxy or castor oil).

Fig. 10 displays the main effect plots for the tensile modulus response, ranging from 3.24 to 5.93 GPa. Switching the matrix phase from castor oil to epoxy polymer results in a notable 36 % increase in terms of tensile modulus (Fig. 10a). As demonstrated in Table 1, a notable difference in tensile modulus exists between synthetic and bio-based polymers, which elucidates why epoxy-based laminates surpass those made with a castor oil matrix. Regarding the reinforcement phase, Fig. 9b illustrates an impressive 83 % increase in tensile modulus when composites are made using UD jute fibres. It is important to note that BD laminates have half the amount of fibres aligned in the load direction compared to UD composites. Moreover, the presence of 90° yarns in the bidirectional fibre architecture induces a shear effect when the 0° yarns are subjected to tension, impeding the transfer of axial loading and consequently reducing the stiffness of the composite. The tensile modulus is more significantly affected by the reinforcement phase factor; as is well established for composite laminates, the tensile properties are largely governed by the fibre characteristics.

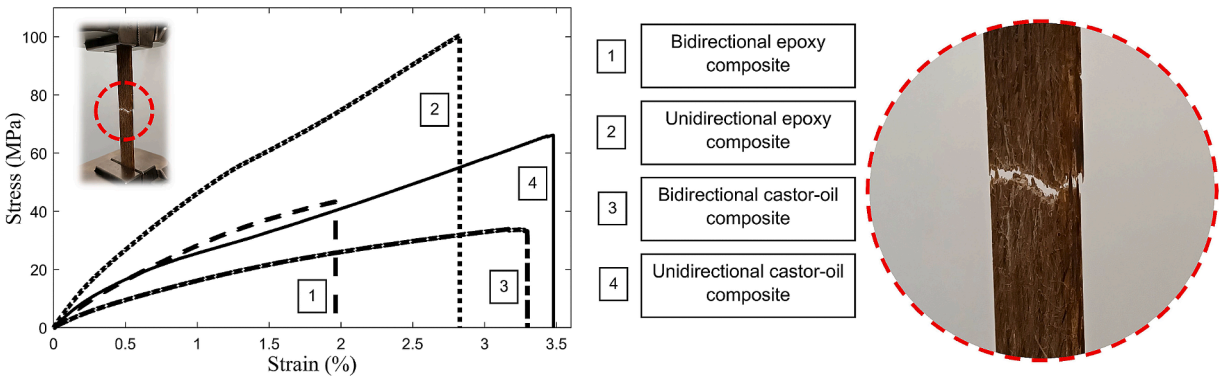

Fig. 11. Typical stress/strain curves and failure for the composite laminates under tensile loads.

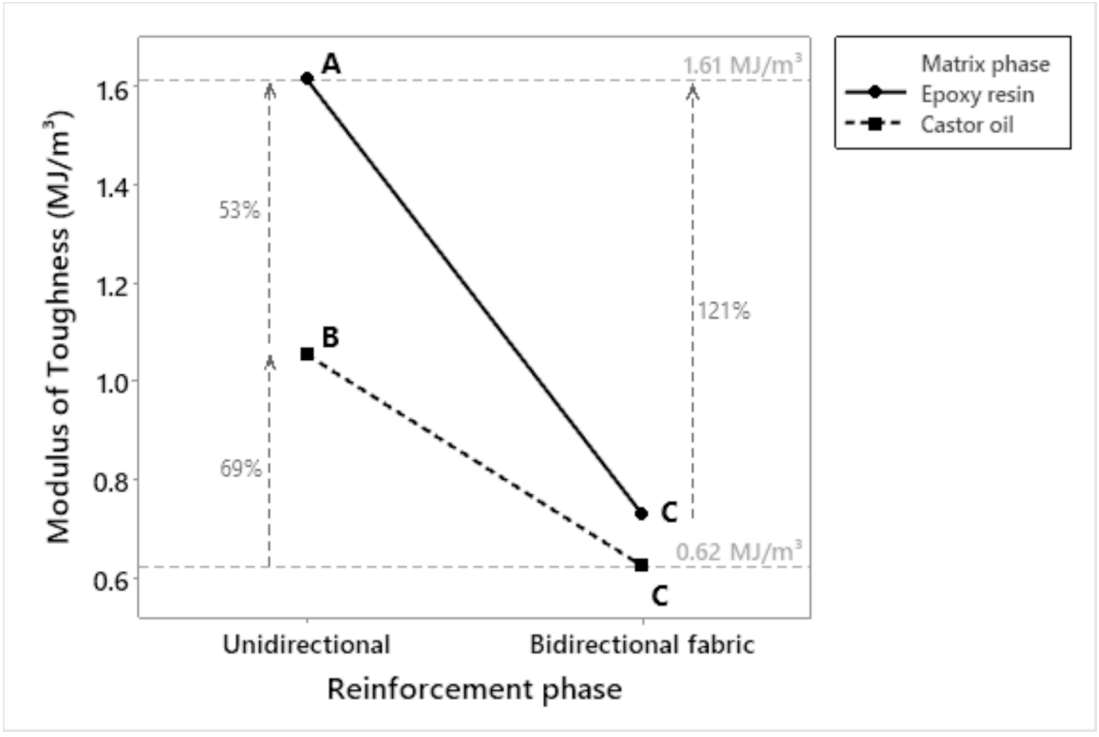

Fig. 12. Second-order interaction effect plot for the mean modulus of toughness.

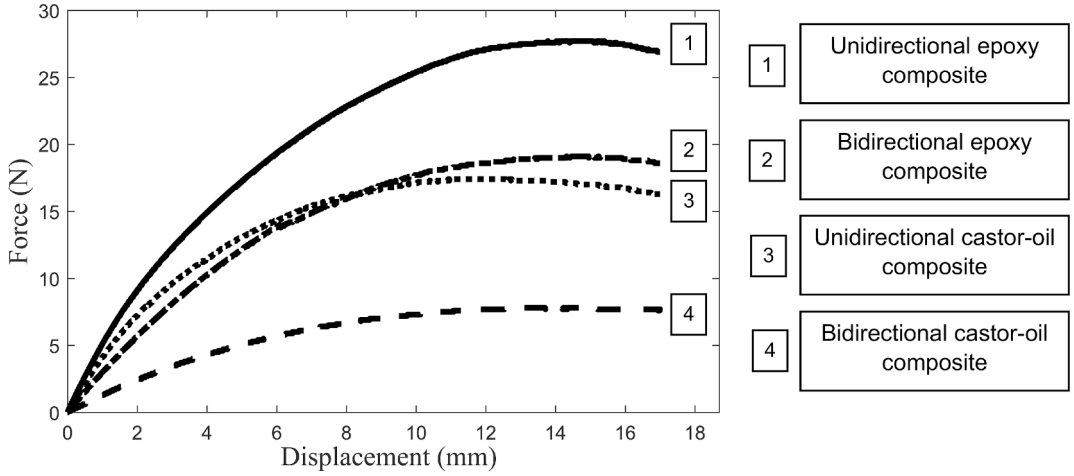

Fig. 13. Typical bending force–displacement curves for the composite materials.

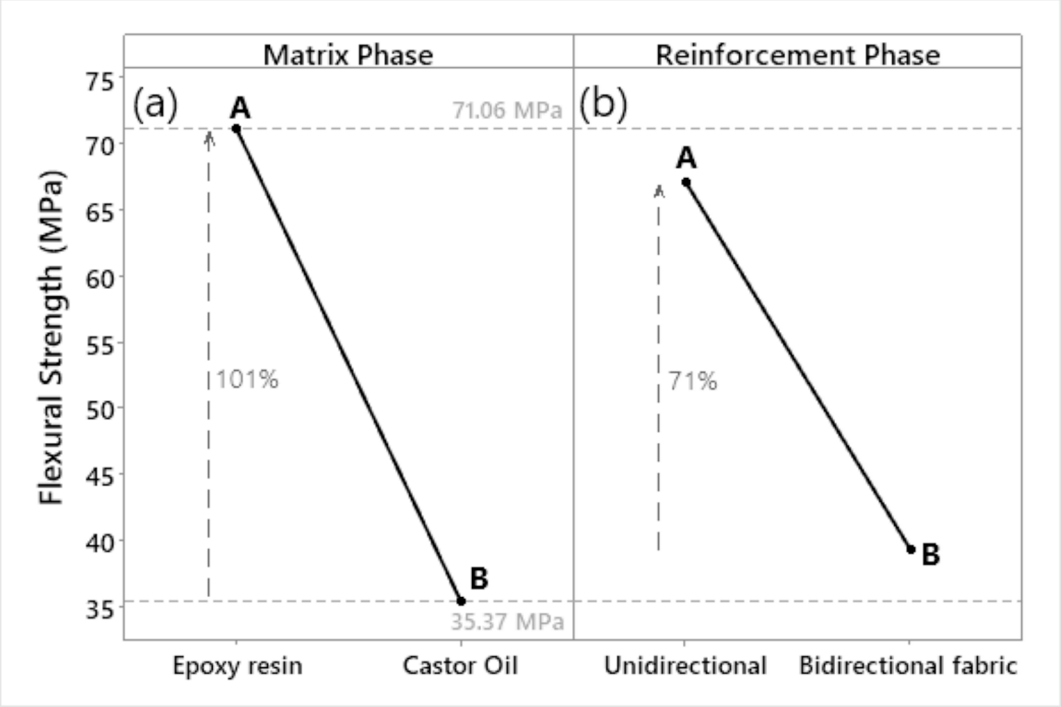

Fig. 14. Effect plots for the mean flexural strength response.

Fig. 11 depicts the typical mechanical behaviour observed in jute fibre composites subjected to tensile loads. All configurations exhibit brittle fracture behaviour and quasi-linear crack propagation, with a full rupture of both phases of the laminates (matrix and fibres), as illustrated in Fig. 11. The modulus of toughness, which measures a material's capacity to absorb energy prior to fracturing, is determined by the area under the stress–strain curve. Additionally, Fig. 12 includes a second-order interaction effect plot for the mean modulus of toughness, which lies between 0.62 to 1.61 MJ/m^3. The results closely resemble the tensile strength behaviour shown in Fig. 9, indicating that composites made with UD jute and epoxy are more effective at energy absorption. Notably, UD jute-epoxy composites (curve 2, Fig. 11) demonstrate approximately 53 % (Fig. 12) higher modulus of toughness compared to UD jute-castor oil composites (curve 4, Fig. 11). Tukey's test reveals no significant difference among the bidirectional jute composites, as they belong to the same letter group C (Fig. 12). The UD architecture for composite laminates surpasses the BD configuration by up to 121 % in terms of modulus of toughness.

3.2.4. *Flexural strength and modulus*

Fig. 13 shows a typical force–displacement curve for each experimental condition measured under the three-point bending test. Like the tensile response, the epoxy composites reinforced with UD jute fibres feature the largest maximum flexural load. Furthermore, a comparable

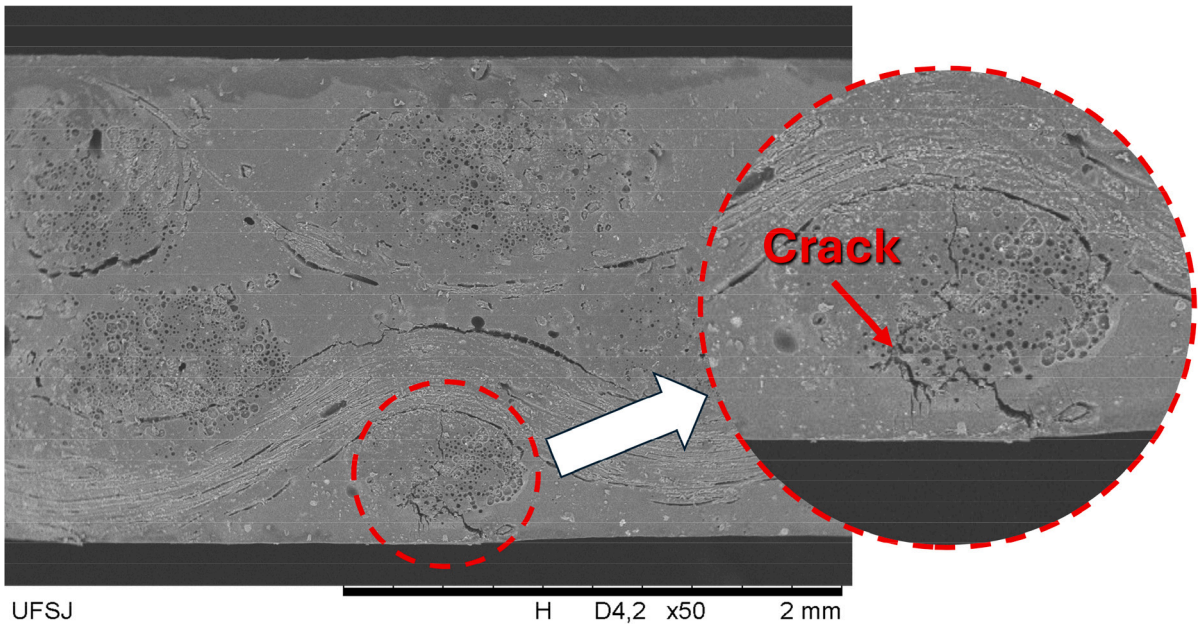

Fig. 15. Micro-cracks propagation in the region under tensile efforts during the three-point bending test of the composite laminates.

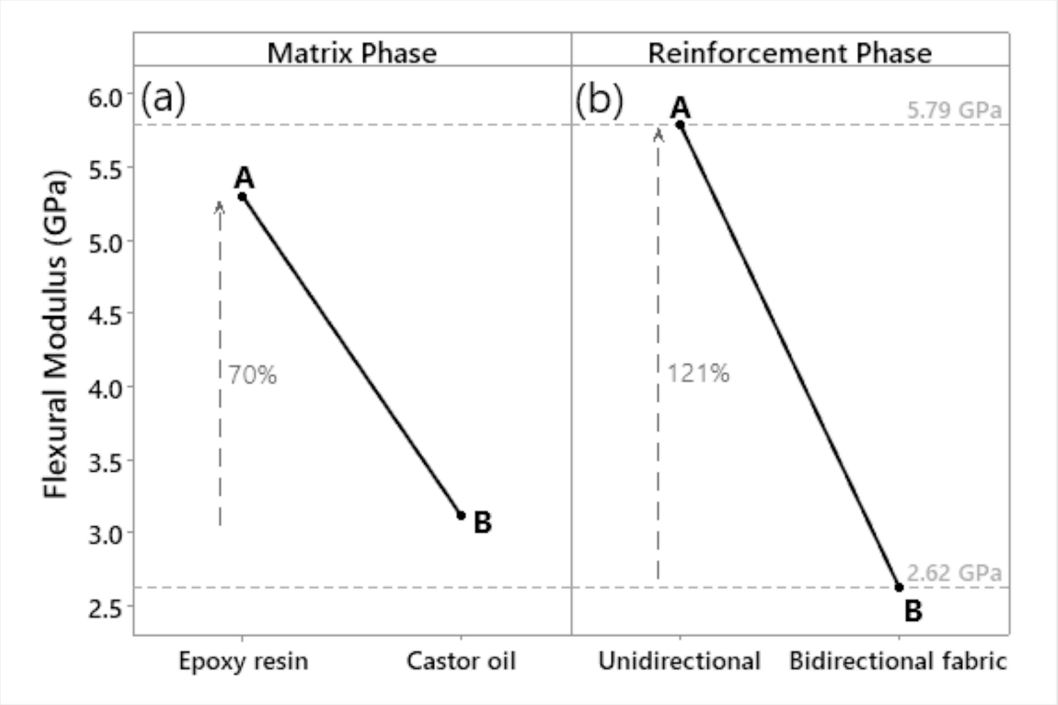

Fig. 16. Effect plots for the mean flexural modulus response.

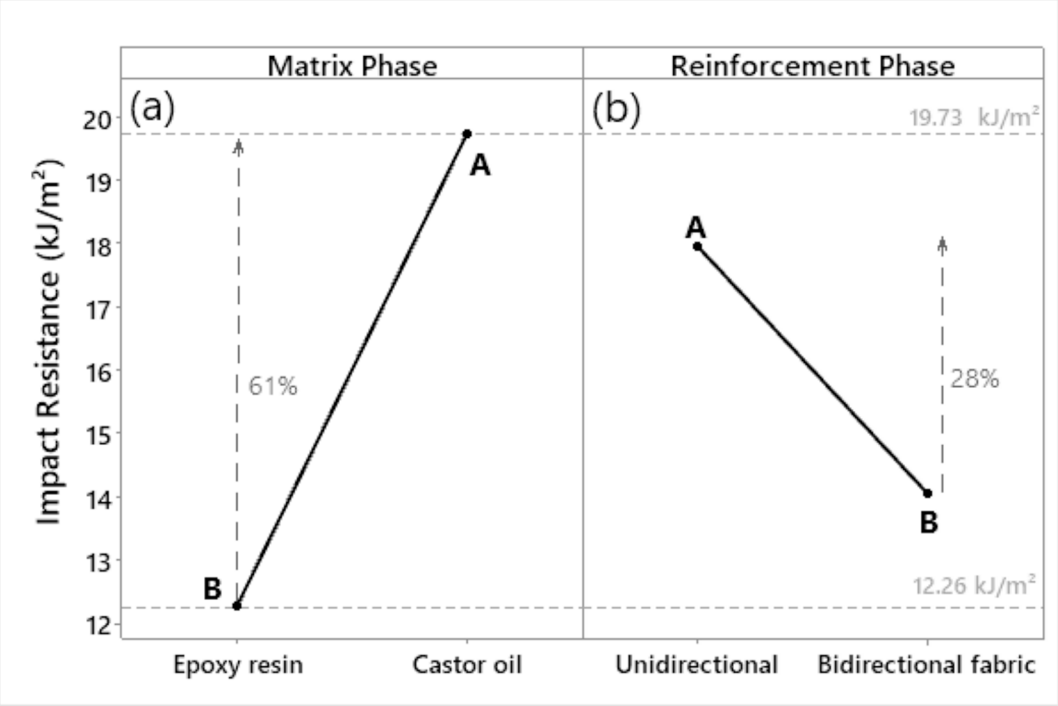

Fig. 17. Main effect plots for the impact resistance.

behaviour is observed between the epoxy-based bidirectional fibre and the castor oil-based UD fibre composites.

In Fig. 14, the main effect plots for the mean flexural strength response of the composite materials are presented, which varies from 35.37 to 71.06 MPa. Epoxy-based composites show a 101 % larger flexural strength than the castor-oil jute fibre composites (Fig. 14a). As previously noted, castor-oil polymer demonstrates lower strength than epoxy polymer (Table 1) and introduces higher porosity when combined with jute fibres (Fig. 7). The three-point bending test combines tensile and compressive efforts in the upper and lower beam sides, respectively. Consequently, the compressive strength of these composites is significantly affected by the properties of the matrix. This contributes to the augmented difference in strength between synthetic (fossil) and bio-based composites under bending, attributed to the lower mechanical performance of the castor-oil polymer. Similarly, the discrepancy between UD and BD jute orientations (Fig. 14b) in comparison to tensile

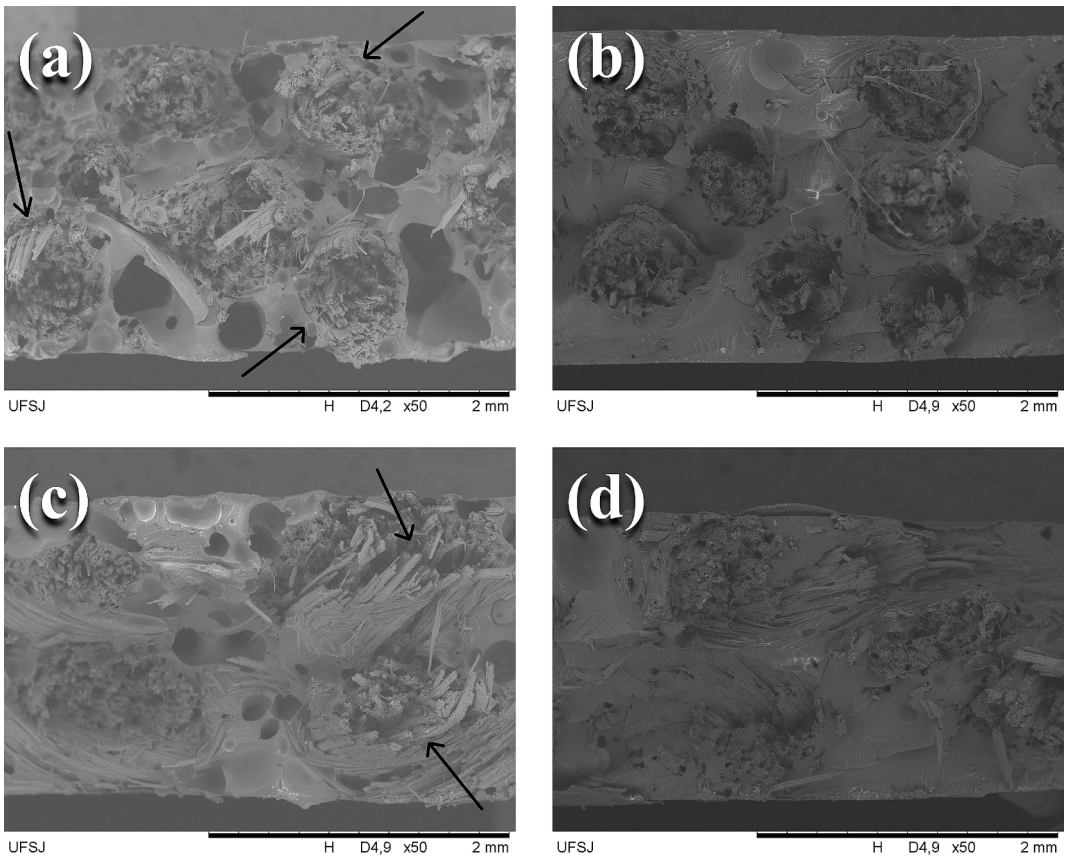

Fig. 18. SEM images of impact fracture surfaces of (a) UD jute castor oil-, (b) UD jute epoxy- (c) bidirectional castor oil-, and (d) bidirectional epoxy-composites.

strength (Fig. 10) is diminished due to the reduced contribution of the fibres under bending. The failure mode of the composite laminates under three-point bending is characterised by micro-cracks in the section experiencing tensile stress, i.e., in the region below the neutral axis – see Fig. 15.

Fig. 16 shows the main effect plots for the mean flexural modulus response, ranging from 2.62 to 5.79 GPa. The disparity in flexural modulus between both factor levels is heightened compared to the tensile effects illustrated in Fig. 10. This behaviour is attributed to the lower mechanical performance of the castor oil polymer, particularly in the upper beam side subjected to compressive efforts. Additionally, as previously mentioned, the transverse orientation of the yarns in the BD laminates decreases the tensile behaviour of the composites (lower beam side), further contributing to the reduction in flexural modulus of the

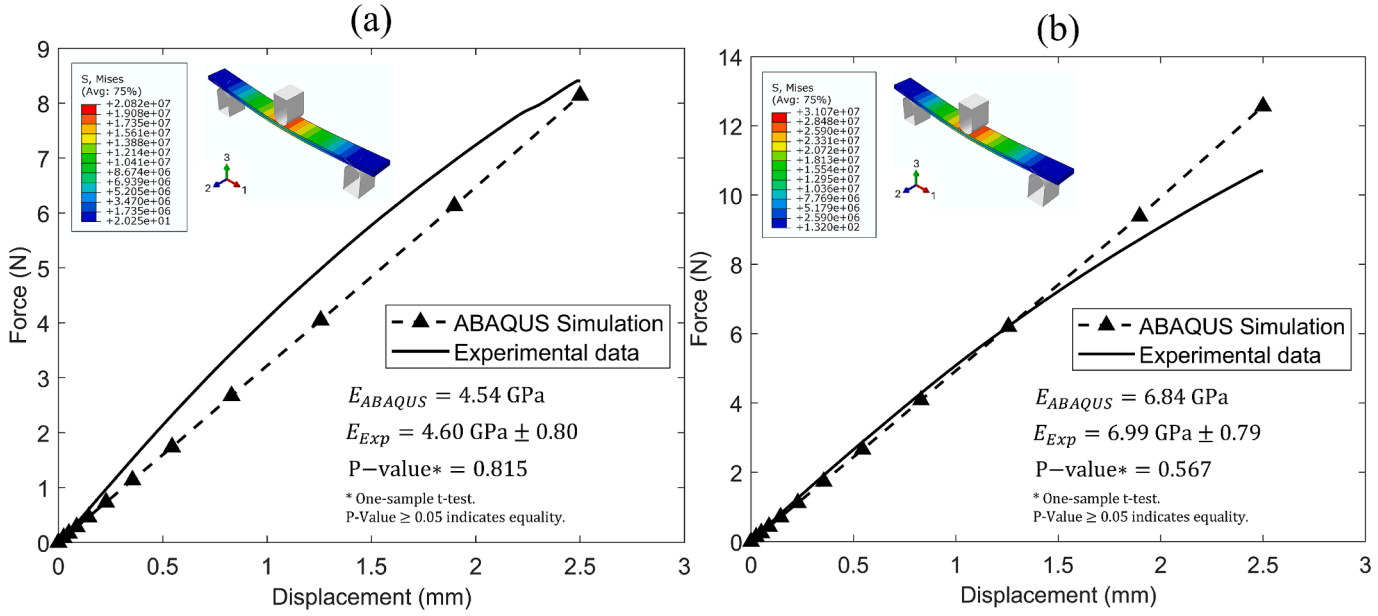

Fig. 19. Numerical and experimental bending force–displacement graphs for UD composites made with castor oil (a) and epoxy (b) polymers.

bidirectional composites.

3.2.5. Impact resistance

Fig. 17 presents the main effect plots for the mean impact resistance response, with values between 12.26 and 19.73 kJ/m^2. In contrast to the tensile and bending behaviours, the castor oil matrix phase demonstrates approximately 61 % greater impact resistance than epoxy composites (Fig. 17a). According to Table 1, the castor oil polymer absorbs nearly 90 % more impact energy than epoxy systems. Fig. 18 displays the SEM images of composite cross-sections following impact testing. The fracture mode in castor oil composites is predominantly influenced by the fibre pull-out mechanism (Fig. 18a, c), which plays a crucial role in dissipating impact energy [20]. In contrast, the epoxy matrix exhibits less fibre pull-out due to its larger interface bonding, which causes the jute yarns to rupture. Furthermore, it is evident that UD orientation provides superior impact resistance compared to the BD configuration (Fig. 17b). This advantage is mainly attributed to the higher number of yarns aligned along the longitudinal direction (Fig. 18a, b), which enhances the fibre pull-out effect and contributes to improved impact performance.

3.3. Finite element analysis

Fig. 19 presents the numerical (ABAQUS simulation) and experimental bending force–displacement curves for UD jute composites made with castor oil (a) and epoxy polymers (b). Additionally, the stress distribution (von Mises) of the finite element (FE) sample at a 2.5 mm displacement is illustrated. A strong correlation is observed between the experimental and numerical curves. The one-sample *t*-test in Minitab is used to determine if the mean of a sample significantly differs from a specified value. In this context, the test is applied to compare the experimental flexural modulus values with the simulated ones. The results indicate that all P-values are greater than 0.05, suggesting no statistically significant differences between the experimental and simulated values. This implies that the experimental data aligns well with the simulations, confirming their accuracy in representing the tested conditions and reinforcing the assumptions of isotropy and anisotropy incorporated in the numerical parameters.

4. Conclusions

Jute yarn fabric composites made from biobased and synthetic polymers were explored as an alternative for manufacturing large components. The individual material phases were characterised, and a finite element (FE) model was developed to predict the bending behaviour of the composites. A statistical design was implemented to assess the effects of polymer and fabric type on the physical and mechanical properties of the composites. The use of castor oil as a matrix phase reduced the apparent density while increasing the apparent porosity of the composites. This castor oil matrix resulted in a decrease in tensile modulus, flexural strength, and flexural modulus, which can be attributed to the higher porosity achieved. In contrast, the biobased polymer demonstrated improved impact resistance compared to the epoxy composites, primarily due to the fibre pull-out effect that more effectively dissipates impact energy. Unidirectional jute fibre yarns as a reinforcing phase led to reduced apparent porosity and enhanced mechanical properties compared to bidirectional fibre orientation, owing to the greater number of fibres oriented in the longitudinal direction. The numerical simulation showed a strong correlation with the experimental results for small displacements (elastic behaviour) under three-point bending. Overall, the composite laminates produced have proven to be a sustainable and economical alternative for secondary structural applications, particularly those manufactured with unidirectional jute fibre yarns.

Credit authorship contribution statement

Paulo Victor de Assis: Investigation, Conceptualisation, Methodology, Resources, Data curation, Formal analysis, Software, Validation, Visualisation, Writing – original draft, Writing – review & editing. **Rodrigo José da Silva:** Conceptualisation, Software, Validation, Visualisation, Writing – review & editing. **Guilherme Germano Braga:** Writing – original draft. **Antônio Ancelotti Junior:** Supervision, Conceptualisation, Writing – review. **Márcio Eduardo Silveira:** Supervision, Conceptualisation, Methodology, Writing – review. **Túlio Hallak Panzera:** Supervision, Conceptualisation, Methodology, Resources, Writing – review & editing. **Fabrizio Scarpa:** Conceptualisation, Writing – review.

Declaration of competing interest

The authors declare the following financial interests/personal relationships which may be considered as potential competing interests: Tulio Hallak Panzera reports equipment, drugs, or supplies was provided by CNPq. Tulio Hallak Panzera reports equipment, drugs, or supplies was provided by Minas Gerais State Foundation of Support to the Research. Fabrizio Scarpa reports equipment, drugs, or supplies was provided by European Research Council. If there are other authors, they declare that they have no known competing financial interests or personal relationships that could have appeared to influence the work reported in this paper..

Acknowledgements

The authors acknowledge for the financial support provided by the Brazilian Research Agencies CNPq (PQ- 305553/2023-2, DT-303160/2023-3) and FAPEMIG (APQ-04336-23); as well as by the European Research Council, Belgium (ERC-2020-AdG 101020715 NEUROMETA, UK).

Data availability

Data will be made available on request.

References

[1] M. F. Ashby, Materials and the Environment: Eco-Informed Material Choice, third ed., Elsevier, 2021. doi: 10.1016/c2016-0-04008-1.
[2] J. A. de Oliveira, D. A. Lopes Silva, F. N. Puglieri, Y. M. B. Saavedra, Life Cycle Engineering and Management of Products, Springer Cham, 2021. doi: 10.1007/978-3-030-78044-9.
[3] Azman MA, et al. Natural Fiber Reinforced Composite Material for Product Design: A Short Review. Polymers 2021;13:12. https://doi.org/10.3390/polym13121917.
[4] Braga GG, et al. Life cycle assessment of fibre metal laminates: an ecodesign approach. Composites, Part C: Open Access 2024;13:100435. https://doi.org/10.1016/j.jcomc.2024.100435.
[5] Shahinur S, Sayeed MMA, Hasan M, Sayem ASM, Haider J, Ura S. Current Development and Future Perspective on Natural Jute Fibers and Their Biocomposites. Polymers 2022;14:7. https://doi.org/10.3390/polym14071445.
[6] Dobah Y, Bourchak M, Bezazi A, Belaadi A, Scarpa F. Multi-axial mechanical characterization of jute fiber/polyester composite materials. Compos B Eng 2016: 450–6. https://doi.org/10.1016/j.compositesb.2015.10.030.
[7] Khondker OA, Ishiaku US, Nakai A, Hamada H. A novel processing technique for thermoplastic manufacturing of unidirectional composites reinforced with jute yarns. Compos A 2006;37:2274–84. https://doi.org/10.1016/j.compositesa.2005.12.030.
[8] Acosta AP, Delucis RA, Amico SC. Hybrid wood-glass and wood-jute-glass laminates manufactured by vacuum infusion. Constr Build Mater 2023;398: 132513. https://doi.org/10.1016/j.conbuildmat.2023.132513.
[9] Flores A, Albertin A, Delucis RA, Amico SC. Mechanical and Hygroscopic Characteristics of Unidirectional Jute/Glass and Jute/Carbon Hybrid Laminates. J Nat Fibers 2023;20:1. https://doi.org/10.1080/15440478.2023.2178586.
[10] Devireddy SBR, Biswas S. Physical and mechanical behavior of unidirectional banana/jute fiber reinforced epoxy based hybrid composites. Polym Compos 2015; 38:1396–403. https://doi.org/10.1002/pc.23706.
[11] Chakraborty I, Chatterjee K. Polymers and Composites Derived from Castor Oil as Sustainable Materials and Degradable Biomaterials: Current Status and Emerging

Trends. Biomacromolecules 2020;21:4639–62. https://doi.org/10.1021/acs.biomac.0c01291.
[12] Santos JC, et al. Sandwich structures of aluminium SKINS and egg-box-shaped cores made with biobased foam and composites. Journal of building engineering 2024;88:109099. https://doi.org/10.1016/j.jobe.2024.109099.
[13] Assis EG, et al. Water aging effects on the flexural properties of fully biobased coir fiber composites. Polym Eng Sci 2023;63:3719–30. https://doi.org/10.1002/pen.26479.
[14] Braga GG, Rosa FA, Santos JC, Pino GG, Panzera TH, Scarpa F. Fully biobased composite and fiber-metal laminates reinforced with Cynodon spp. fibers. Polym Compos 2023;44:453–64. https://doi.org/10.1002/pc.27109.
[15] Vial ED, et al. Glass and Aramid Fibre-reinforced Bio-based Polymer Composites Manufactured By Vacuum Infusion: A Statistical Approach to Their Physical and Mechanical Properties. Appl Compos Mater 2023;30:1627–44. https://doi.org/10.1007/s10443-023-10142-8.
[16] Napolitano F, Santos JC, da Silva RJ, Braga GG, Freire RTS, Panzera TH. Sandwich panels made of aluminium skins and gapped-bamboo ring core. J Braz Soc Mech Sci Eng 2023;45:250. https://doi.org/10.1007/s40430-023-04140-x.
[17] Oliveira LÁ, Tonatto MLP, Coura GLC, Freire RTS, Panzera TH, Scarpa F. Experimental and numerical assessment of sustainable bamboo core sandwich panels under low-velocity impact. Constr Build Mater 2021;292:123437. https://doi.org/10.1016/j.conbuildmat.2021.123437.
[18] Oliveira P, Kilchert S, May M, Panzera T, Scarpa F, Hiermaier S. Numerical and experimental investigations on sandwich panels made with eco-friendly components under low-velocity impact. J Sandw Struct Mater 2021;24:419–47. https://doi.org/10.1177/10996362211020428.
[19] Junqueira DM, Gomes GF, Silveira ME, Ancelotti AC. Design Optimization and Development of Tubular Isogrid Composites Tubes for Lower Limb Prosthesis. Appl Compos Mater 2018;26:273–97. https://doi.org/10.1007/s10443-018-9692-2.
[20] Oliveira LÁ, Santos JC, Panzera TH, Freire RTS, Vieira LMG, Scarpa F. Evaluation of hybrid-short-coir-fibre-reinforced composites via full factorial design. Compos Struct 2018;202:313–23. https://doi.org/10.1016/j.compstruct.2018.01.088.
[21] D. C. Montgomery, G.C. Runger. Applied Statistics and Probability for Engineers, Wiley, 7th edition, July 8, 2020.
[22] Daniel IM, Ishai O. Engineering mechanics of composite materials. 2nd edition,. New York: Oxford University Press; 2006.
[23] ASTM D3822-14: 2020. Standard Test Method for Tensile Properties of Single Textile Fibers.
[24] ASTM D3039/D3039M-17:2017. Standard test method for tensile properties of polymer matrix composite materials.
[25] ASTM D790-17:2017. Standard test methods for flexural properties of unreinforced and reinforced plastics and electrical insulating materials.
[26] ASTM D6110-18:2018. Standard test method for determining the charpy impact resistance of notched specimens of plastics.
[27] BS EN ISO 10545-3:2018. Part 3: Determination of water absorption, apparent porosity, apparent relative density and bulk density.
[28] R.J. da Silva et al., Enhanced core rigidity classifier method (RJS 2.0): a comprehensive approach to properly measure elastic properties of sandwich structures, Composite Structures, pp. 117981–117981, Feb. 2024, doi: 10.1016/j.compstruct.2024.117981.
[29] ASTM D3518-18:2018 Standard Test Method for In-Plane Shear Response of Polymer Matrix Composite Materials by Tensile Test of a ±45° Laminate.
[30] Smail YB, El Moumen A, Imad A, Lmai1 F, Ezahri M. Effect of heat treatment on the mechanical properties of jute yarns. J Compos Mater 2021;55:2777–92. https://doi.org/10.1177/0021998321999103.
[31] Shi J, Yuan S, Zhang W, Wang G, Zhang J, Chen H, et al. Jute yarn-wound composites: optimization of methods for evaluating mechanical properties and improvement of mechanical properties. J Mater Res Technol 2022;21:827–40. https://doi.org/10.1016/j.jmrt.2022.09.076.
[32] Tripathy SS, Di Landro L, Fontanelli D, Marchetti A, Levita G. Mechanical properties of jute fibers and interface strength with an epoxy resin. J Appl Polym Sci 2000;75:1585–96. https://doi.org/10.1002/(SICI)1097-4628(20000328)75:13<1585::AID-APP4>3.0.CO;2-Q.
[33] Biswas S, Ahsan Q, Verpoest I, Hasan M. Effect of Span Length on the Tensile Properties of Natural Fibers. Adv Mat Res 2011;264–265:445–50. https://doi.org/10.4028/www.scientific.net/amr.264-265.445.
[34] Defoirdt N, et al. Assessment of the tensile properties of coir, bamboo and jute fibre. Compos A Appl Sci Manuf 2010;41(5):588–95. https://doi.org/10.1016/j.compositesa.2010.01.005.
[35] M. E. A. Fidelis et al. The effect of fiber morphology on the tensile strength of natural fibers, Journal of Materials Research and Technology, vol. 2, no. 2, pp. 149–157, Apr. 2013, doi: 10.1016/j.jmrt.2013.02.003.